

NEURAL OPERATOR WITH REGULARITY STRUCTURE FOR MODELING DYNAMICS DRIVEN BY SPDES

Peiyan Hu^{1*}, Qi Meng^{2†}, Bingguang Chen³, Shiqi Gong³, Yue Wang², Wei Chen³, Rongchan Zhu⁴, Zhi-Ming Ma³, Tie-Yan Liu²

¹University of Chinese Academy of Sciences, ²Microsoft Research Asia

³Chinese Academy of Sciences, ⁴Bielefeld University

ABSTRACT

Stochastic partial differential equations (SPDEs) are significant tools for modeling dynamics in many areas including atmospheric sciences and physics. Neural Operators, generations of neural networks with capability of learning maps between infinite-dimensional spaces, are strong tools for solving parametric PDEs. However, they lack the ability to modeling SPDEs which usually have poor regularity¹ due to the driving noise. As the theory of regularity structure has achieved great successes in analyzing SPDEs and provides the concept *model feature vectors* that well-approximate SPDEs' solutions, we propose the Neural Operator with Regularity Structure (NORS) which incorporates the feature vectors for modeling dynamics driven by SPDEs. We conduct experiments on various of SPDEs including the dynamic Φ_1^4 model and the 2d stochastic Navier-Stokes equation, and the results demonstrate that the NORS is resolution-invariant, efficient, and achieves one order of magnitude lower error with a modest amount of data.

1 INTRODUCTION

Stochastic partial differential equations (SPDEs) are significant tools for modeling dynamics in many areas including atmospheric sciences (Hasselmann, 1976), physics (Uhlenbeck & Ornstein, 1930), biology (Wilkinson, 2018), economics (Barone-Adesi & Whaley, 1987), etc. SPDEs generalize partial differential equations via random force terms and they are used to study statistical mechanics of the dynamics systems. Examples include stochastic Navier-Stokes equations modeling the statistics of turbulent flows (Buckmaster & Vicol, 2019) in atmospheric science and the Φ^4 model arising in the stochastic quantisation of quantum field theory (Hairer, 2015). Since SPDEs relate to many scientific open problems, studying the solution of SPDEs from both mathematical proving and numerical methods is a hot research direction in both math and physics.

Inspired by recent advances in using AI techniques to accelerate scientific computing, we study using deep learning method for modeling the solution of SPDEs. There have been deep learning models arising for modeling dynamics governed by PDE such as Neural Operators (Kovachki et al., 2021), DeepONet (Lu et al., 2019), which model the map between infinite-dimensional functions and agree with the case of learning solutions of a family of parametric PDEs. However, SPDEs usually have poor regularity w.r.t the time variable for function-valued noise and singularity w.r.t space for space-time white noise that these models do not take into consideration. Thus, they cannot accurately represent the solution of the SPDE.

To deal with the singularity of SPDEs, we incorporate the regularity structure theory (Hairer, 2014) with neural operator to model the map between (initial condition, driving noise) to the solution. The key step is to project the driving noise and initial conditions to the *model feature vectors* in regularity structure theory which improves the regularity according to the regularity structure theory.

Our Contributions We introduce the Neural Operator with Regularity Structure (NORS) that extends the Neural Operators. This deep-learning-based method has four advantages as follows: (1)

*This work was done when the first author was visiting Microsoft Research Asia.

†Corresponding E-mail: meq@microsoft.com.

¹Roughly speaking, regularity describes the smoothness of a function.

The NORS can solve equations whose initial conditions and driving force change and are inputted simultaneously, which is beyond the Neural Operators' capability because of its requirement of regularity. The detailed theory about regularity structure is provided in Section 3. (2) The NORS utilizes more information from the equations themselves as we take models as our features, which contain the information of the SPDEs' differential operators and then leads to lower loss. (3) The NORS inherits Neural Operators' zero-shot super-resolution, which means it does not need a large amount of data and is mesh-invariant. We test the NORS on the dynamic Φ_1^4 model, reaction-diffusion equation with linear multiplicative noise and the 2d stochastic Navier-Stokes equation. Using the NORS, both the testing accuracy and sample complexity are enhanced. Specifically, the error is one order of magnitude lower than other baselines.

2 RELATED WORK

There have been several popular deep-learning-based methods for modeling the solution of parametric partial differential equations (Lu et al., 2019; Patel et al., 2021; Kovachki et al., 2021; Li et al., 2020b; Bhattacharya et al., 2020; Nelsen & Stuart, 2021; Li et al., 2020a). For example, the Neural Operator (Kovachki et al., 2021) and Fourier Neural Operator (FNO) (Li et al., 2020b) are representatives which are mesh-independent model, whose architectures approximate Picard iteration for solving PDEs. Since the solution of SPDEs is determined by both the initial condition and the force, capturing the structure of the force (e.g., the space-time white noise) is beyond the capability of these models. To handle the case that SPDEs' solutions depend simultaneously on the initial condition u_0 and the force term ξ , Salvi & Lemercier (2021) introduce the neural stochastic partial differential equation (Neural SPDE), which parameterizes the kernels according to Duhamal's fix-point formula for SPDE whose linear differential operators can generate semigroups. In this paper, we adopt another way which first projects the initial condition and force to a set of models. Since the *models* incorporate more prior (including the kernel, the initial condition, and the force) of the SPDE, it is expected to have a better generalization and lower sample complexity.

3 PRELIMINARY

In this section, we introduce background on the regularity structure theory (Hairer, 2014) of SPDEs. Consider an SPDE on $[0, T] \times D$ with the following form

$$\begin{aligned} \partial_t u - \mathcal{L}u &= \mu(u, \partial_1 u, \dots, \partial_d u) + \sigma(u, \partial_1 u, \dots, \partial_d u)\xi, \\ u(0, x) &= u_0(x), \end{aligned} \quad (1)$$

where $x \in D \subset \mathbb{R}^d$, $t \in [0, T]$, \mathcal{L} is a linear differential operator, ξ is the space-time white noise, $u_0 : D \rightarrow \mathbb{R}$ is the initial condition. Under local Lipschitz condition on μ, σ with respect to suitable norm, this SPDE has a unique mild solution (Hairer, 2014; Salvi & Lemercier, 2021):

$$u_t = e^{t\mathcal{L}}u_0 + \int_0^t e^{(t-s)\mathcal{L}}\mu(u_s, \partial_1 u_s, \dots, \partial_d u_s)ds + \int_0^t e^{(t-s)\mathcal{L}}\sigma(u_s, \partial_1 u_s, \dots, \partial_d u_s)\xi ds. \quad (2)$$

Thus in the field of SPDE, the solution is determined by both the initial condition and the force term, i.e., $(u_0, \xi) \mapsto u$. The design of deep learning models such as Neural Operators does not consider the solution structure of SPDE, therefore, they cannot well approximate the case $(u_0, \xi) \mapsto u$.

It is then natural to utilize the regularity structure theory to help handle the regularity problem. The concept *model* in the regularity structure is a collection of *model feature vectors*, which are multi-dimensional signals designed to approximate solutions of SPDEs even with low regularity regimes. The motivation comes from Picard theorem and Taylor expansion. According to the representation of the mild solution in Eqn.(2), we define two linear operators $I[f](t) = \int_0^t e^{(t-s)\mathcal{L}}f(s)ds$ and $I_c[u_0](t) = e^{t\mathcal{L}}u_0$ for any function f defined on $[0, T] \times D$ to \mathbb{R}^d . Picard theorem shows that the following recursive sequence approximates the solution u of equation (1) as $n \rightarrow \infty$

$$u_t^0 = I_c[u_0]_t, \quad u_t^{n+1} = I_c[u_0]_t + I[\mu(u^n) + \sigma(u^n)\xi]_t. \quad (3)$$

Using Taylor expansion, we then have the recursive sequence that can approximate u as $m, l, n \rightarrow \infty$

$$\begin{aligned} u_t^{0,m,l} &= I_c[u_0]_t, \\ u_t^{n+1,m,l} &= I_c[u_0]_t + \sum_{k=0}^m \frac{\mu^{(k)}(0)}{k!} I[(u^{n,m,l})^k]_t + \sum_{k=0}^l \frac{\sigma^{(k)}(0)}{k!} I[(u^{n,m,l})^k \xi]_t. \end{aligned} \quad (4)$$

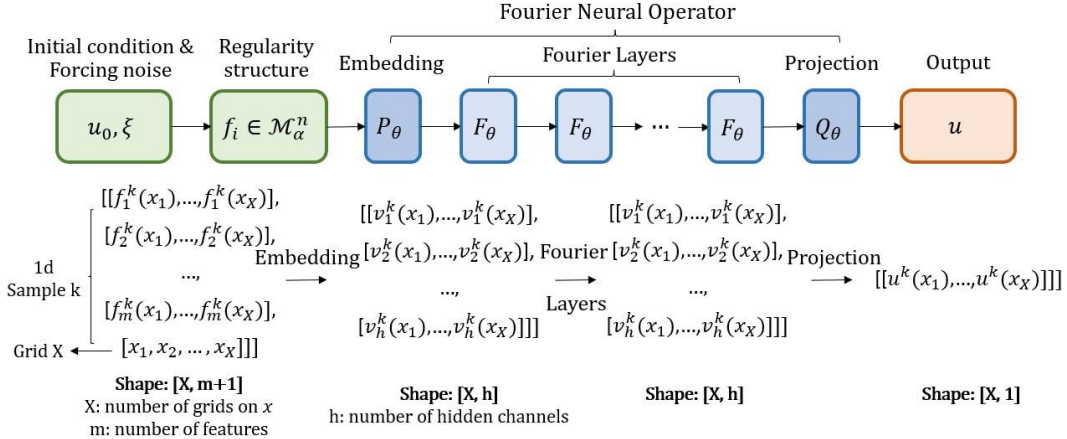


Figure 1: The architecture of our model and the shape of the data of one sample in the 1d case.

Then, the solution of SPDE can be approximated by weighted sum of the features $I[(u^{n,m,l})^k], I[(u^{n,m,l})^k], l = 0, \dots, k; m = 0, \dots, k$, where we call n as the height and m, l as the width in the approximation. Motivated by this, Chevyrev et al. (2021) develops tool for feature engineering of SPDEs. By the regularity structure theory, the model feature vectors are obtained by integrals of functionals of u_0 and ξ (as I and I_c are convolution operations), whose regularity is proved to be better due to the polishing effect of integrals (Salvi & Lemercier, 2021). To avoid the number of model feature vectors grows exponentially, the *height* of the features is constrained according to the regularity of the SPDE. Please refer the details about the generation of model feature vectors and its degree constraints in Appendix A.1

4 LEARNING SPDE SOLUTION VIA MODEL FEATURE VECTORS

We move on to introducing the Neural Operator with Regularity Structure (abbrev. NORS). For given SPDE which has the form in Eqn.(1), our goal is to learn its solution solution u_T at given time point T under initial condition u_0 which is assumed to be generated by a parametric distribution. According to Eqn. (3) and (4), the solution depends continuously on the model feature vectors not on the (u_0, ξ) . Therefore, NORS first maps (u_0, ξ) to the model feature vectors, and then we use Fourier Neural Operator (abbrev. FNO) to learn the continuous map from the model feature vectors to the solution.

To represent the continuous input functions u_0 and ξ , we discretize the space-time domain $D \times [0, T]$ with $D \subset \mathbb{R}^d$ onto the grid $O_{X_1} \times \dots \times O_{X_d} \times O_T$. Then we use the values of the continuous function on the grid points to represent them. For one sample of u_0 and ξ , we first get the model feature vectors \mathcal{M} of (u_0, ξ) according to data and the form of the equation. As $\mathcal{M} = \{f_i\}_{i=1, \dots, m}$ are set of continuous functions, we also use its value on discrete grids to represent them. By concatenating all the model feature vectors f_i and the grid $O_{X_1} \times \dots \times O_{X_d}$, we get the inputs w^0 .

Then, w^0 is fed into the FNO and the forward process is expressed as

$$v^0(x) = P_{\theta_{in}}(w^0(x)); \quad v^{i+1}(x) = F_{\theta_i}(v^i(x)); \quad \hat{u}_T(x) = Q_{\theta_{out}}(v^K(x)) \quad (5)$$

for any $x \in D$, where $\theta_{in}, \theta_{out}, \theta_i, i = 0, \dots, K-1$ are learnable weights, $P_{\theta_{in}} : \mathbb{R}^{X_1 \times \dots \times X_d \times (m+d)} \rightarrow \mathbb{R}^{X_1 \times \dots \times X_d \times h}$ be an embedding neural network to project the input to the latent feature space, $F_{\theta_i} : \mathbb{R}^{X_1 \times \dots \times X_d \times h} \rightarrow \mathbb{R}^{X_1 \times \dots \times X_d \times h}$ be a Fourier layer (Li et al., 2020b) which approximates the iteration in Picard's iteration, $Q_{\theta_{out}} : \mathbb{R}^{X_1 \times \dots \times X_d \times h} \rightarrow \mathbb{R}^{X_1 \times \dots \times X_d \times d}$ be a embedding layer to project the latent feature to the output. Here, X_i is the number of grids on dimension x_i , h is the number of hidden channels, and m (the number of model feature vectors) and d (the dimension of region D) are defined before. Since only the FNO contains trainable weights, defining loss function between $\hat{u}_T(x)$ and the groundtruth $u(x)$ can guide the optimization to learn the weights of FNO. A demonstration of our model is shown in Figure 1.

Table 1: **Dynamic Φ_1^4 model.** We consider the $l2$ error of the baselines and our model($n = 2$ or 3) in two settings with training data size $N = 1000$ or 10000 .

Model	$N = 1000$		$N = 10000$	
	$\xi \mapsto u$	$(u_0, \xi) \mapsto u$	$\xi \mapsto u$	$(u_0, \xi) \mapsto u$
FNO	0.032	0.030	0.027	0.024
NSPDE	0.009	0.012	0.006	0.006
Ours($n = 3$)	0.0003	0.0011	0.0002	0.0004
Ours($n = 2$)	0.0002	0.0012	0.0002	0.0004

5 EXPERIMENT

We compare the NORS with other baselines on some significant equations. What we care about includes the $l2$ error on two settings: in the setting $(\xi \mapsto u)$, the noise ξ changes while the initial condition u_0 is fixed; in the setting $((u_0, \xi) \mapsto u)$, both ξ and u_0 vary across samples. We note that in the following equations, we only consider periodic boundary conditions, but Dirichlet or Neumann boundary conditions can also be easily complemented. To save space, the details about the construction of the model \mathcal{M} of each SPDE are put into Appendix A.1. We use 32 hidden channels and 4 Fourier layers for our NORS in all experiments. We use the Adam optimizer to train for 500 epochs with an initial learning rate of 0.001 in the first two experiments and and the 2d stochastic Navier-Stokes equation on 64×64 grid, and 0.01 for the 2d stochastic Navier-Stokes equation on 16×16 grid (after grid search) that are halved every 100 epochs. We randomly split the dataset into training and test sets by 5:1. The NORS codes are deposited in GitHub at <https://github.com/Peiyannn/Neural-Operator-with-Regularity-Structure.git>.

5.1 DYNAMIC Φ_1^4 MODEL

We first consider the dynamic Φ_1^4 model with the periodic boundary condition. It takes the form

$$\begin{aligned} \partial_t u - \Delta u &= 3u - u^3 + \xi, \quad (t, x) \in [0, 0.05] \times [0, 1] \\ u(t, 0) &= u(t, 1), \quad (\text{Periodic BC}) \\ u_0(x) &= u(0, x) = x(1 - x) + \kappa\eta(x), \end{aligned} \tag{6}$$

where ξ is the space-time white noise, $\eta(x) = \sum_{k=-10}^{k=10} \frac{a_k}{1+|k|^2} \sin(\lambda^{-1}k\pi(x - 0.5))$, with $a_k \sim \mathcal{N}(0, 1)$ with $\lambda = 2$, and $\kappa = 0$ or 0.1 corresponding to the initial condition is fixed or not.

For this equation, the differential operator \mathcal{L} is Δ , according to which the operator I and I_c of the model \mathcal{M}^n is given by $I[f](t) = \int_0^t e^{(t-s)\Delta} f(s) ds$ and $I_c[u_0](t) = e^{t\Delta} u_0$, where Δ is the Laplace operator on D and $f : [0, T] \times D \rightarrow \mathbb{R}$.

The result is shown in Table 1. We consider two settings, in both of which our architecture outperforms other benchmarks a lot. Even compared with the lowest error of all baselines, our result is about a tenth of it in the $(u_0, \xi) \mapsto u$ setting, while the result of $\xi \mapsto u$ setting is even better. We also note that our model can perform well with few data and low height.

5.2 REACTION-DIFFUSION EQUATION WITH LINEAR MULTIPLICATIVE FORCING

As the dynamic Φ_1^4 model is a parabolic equation with additive forcing, we then consider a parabolic equation with multiplicative forcing, which is given by

$$\begin{aligned} \partial_t u - \Delta u &= 3u - u^3 + u\xi, \quad (t, x) \in [0, 0.05] \times [0, 1] \\ u(t, 0) &= u(t, 1), \quad (\text{Periodic BC}) \\ u_0(x) &= u(0, x) = x(1 - x) + \kappa\eta(x), \end{aligned} \tag{7}$$

where ξ is the space-time white noise, and $\eta(x)$ is the same as the Φ_1^4 model. As the form of the operator I and I_c of this equation is the same as the Φ_1^4 model, the model \mathcal{M}^n can be constructed similarly. Please check the details in Appendix A.1.

Table 2: **Reaction-Diffusion equation with linear multiplicative forcing.** We compare the $l2$ error of the baselines and our model($n = 2$ or 3) with training data size $N = 1000$ or 10000 .

Model	$N = 1000$		$N = 10000$	
	$\xi \mapsto u$	$(u_0, \xi) \mapsto u$	$\xi \mapsto u$	$(u_0, \xi) \mapsto u$
FNO	0.0036	0.0063	0.0035	0.0037
NSPDE	0.0016	0.0062	0.0012	0.0026
Ours($n = 3$)	0.0006	0.0005	0.0005	0.0003
Ours($n = 2$)	0.0006	0.0006	0.0005	0.0003

Table 3: **2d stochastic Navier-Stokes equation.** We compare the $l2$ error of the baselines and our model($n = 2$ or 3) in two settings with 1000 training samples. While solving the equation on 64×64 grid, we train the model on 64×64 and 16×16 grid respectively.

Model	64×64 grid		16×16 grid	
	$\xi \mapsto \omega$	$(\omega_0, \xi) \mapsto \omega$	$\xi \mapsto \omega$	$(\omega_0, \xi) \mapsto \omega$
NSPDE	0.039	0.031	0.074	0.063
Ours($n = 3$)	0.0017	0.0029	0.0020	0.0034
Ours($n = 2$)	0.0018	0.0028	0.0022	0.0030

The results in Table 2 show that our model has one order of magnitude lower error in both of the two settings. The experiments on the two equations clearly show that the effectiveness of the *model feature vectors* and the worse generalization of FNO on SPDEs.

5.3 2D STOCHASTIC NAVIER-STOKES EQUATION

As both NSPDE and our model claim mesh-invariance, we evaluate both the $l2$ error and the mesh-invariance property of NSPDE and our model on a 2d Navier-Stokes equation for an incompressible flow:

$$\partial_t w - \nu \Delta w = -u \cdot \nabla w + f + \sigma \xi, \quad (t, x) \in [0, 0.05] \times [0, 1]^2 \quad (8)$$

$$\omega(0, x) = \omega_0(x) \quad (9)$$

where u is the velocity field, $\omega = \nabla \times u$ is the vorticity, ω_0 is the initial vorticity, f is the deterministic force defined as in (Li et al., 2020b), ξ is the random force rescaled by $\sigma = 0.05$ defined as in (Salvi & Lemercier, 2021), and the viscosity parameter $\nu = 10^{-4}$.

Our target is to model the vorticity ω , which is harder to learn compared with the velocity u . According to the form of the equation, the operation I and I_c in model \mathcal{M}^n is defined as $I[f](t) = \int_0^t e^{(t-s)\nu\Delta} f(s) ds$ and $I_c[\omega_0](t) = e^{t\nu\Delta} \omega_0$, where Δ is the Laplace operator defined on the 2d space. While solving the 2d Navier-Stokes equation on 64×64 grid, we train the model on 64×64 and 16×16 grid respectively to test the mesh-invariant property of our model. We follow the data generation process in (Salvi & Lemercier, 2021) to generate the ground-truth for training.

As shown in Table 3, the error of our model is one order of magnitude lower in the $\xi \mapsto \omega$ and $(\omega_0, \xi) \mapsto \omega$ settings. Besides, we solve the equation on 64×64 grid, then train on the 64×64 grid and 16×16 grid. From the results, we verify the resolution-invariance of our model.

6 CONCLUSION AND FUTURE WORK

In this work, we introduce NORS as a strong SPDE-solving tool with the zero-shot super-resolution property. By incorporating the regularity structure, the NORS absorbs both the advantages of Neural Operators and regularity structure, and makes up for the shortcomings. Not only can the NORS learn solution operators $(u_0, \xi) \mapsto u$ of SPDEs, but also has a much lower error. In the future, as the NORS requires that the differential operator \mathcal{L} is already known, we can extend this method by parameterizing the kernel, which will be able to handle the inverse problem that some part of the equations is unknown.

REFERENCES

Giovanni Barone-Adesi and Robert E Whaley. Efficient Analytic Approximation of American Option Values. *Journal of Finance*, 42(2):301–320, June 1987. URL <https://ideas.repec.org/a/bla/jfinan/v42y1987i2p301-20.html>.

Kaushik Bhattacharya, Bamdad Hosseini, Nikola B Kovachki, and Andrew M Stuart. Model reduction and neural networks for parametric pdes. *arXiv preprint arXiv:2005.03180*, 2020.

Tristan Buckmaster and Vlad Vicol. Convex integration and phenomenologies in turbulence. 2019.

Ilya Chevyrev, Andris Gerasimovics, and Hendrik Weber. Feature engineering with regularity structures. 2021.

M. Hairer. A theory of regularity structures. *Invent. Math.*, 198(2):269–504, 2014.

Martin Hairer. Regularity structures and the dynamical ϕ_3^4 model. 2015.

K. Hasselmann. Stochastic climate models part i. theory. *Tellus*, 28(6):473–485, 1976. doi: 10.3402/tellusa.v28i6.11316. URL <https://doi.org/10.3402/tellusa.v28i6.11316>.

Nikola B. Kovachki, Zongyi Li, Burigede Liu, Kamyar Azizzadenesheli, Kaushik Bhattacharya, Andrew M. Stuart, and Anima Anandkumar. Neural operator: Learning maps between function spaces. *CoRR*, abs/2108.08481, 2021. URL <https://arxiv.org/abs/2108.08481>.

Zongyi Li, Nikola Kovachki, Kamyar Azizzadenesheli, Burigede Liu, Andrew Stuart, Kaushik Bhattacharya, and Anima Anandkumar. Multipole graph neural operator for parametric partial differential equations. *Advances in Neural Information Processing Systems*, 33:6755–6766, 2020a.

Zongyi Li, Nikola B. Kovachki, Kamyar Azizzadenesheli, Burigede Liu, Kaushik Bhattacharya, Andrew M. Stuart, and Anima Anandkumar. Fourier neural operator for parametric partial differential equations. *CoRR*, abs/2010.08895, 2020b. URL <https://arxiv.org/abs/2010.08895>.

Lu Lu, Pengzhan Jin, and George Em Karniadakis. Deepnet: Learning nonlinear operators for identifying differential equations based on the universal approximation theorem of operators. *arXiv preprint arXiv:1910.03193*, 2019.

Nicholas H Nelsen and Andrew M Stuart. The random feature model for input-output maps between banach spaces. *SIAM Journal on Scientific Computing*, 43(5):A3212–A3243, 2021.

Ravi G Patel, Nathaniel A Trask, Mitchell A Wood, and Eric C Cyr. A physics-informed operator regression framework for extracting data-driven continuum models. *Computer Methods in Applied Mechanics and Engineering*, 373:113500, 2021.

Cristopher Salvi and Maud Lemercier. Neural stochastic partial differential equations. *CoRR*, abs/2110.10249, 2021. URL <https://arxiv.org/abs/2110.10249>.

G. E. Uhlenbeck and L. S. Ornstein. On the theory of the brownian motion. *Phys. Rev.*, 36:823–841, Sep 1930. doi: 10.1103/PhysRev.36.823. URL <https://link.aps.org/doi/10.1103/PhysRev.36.823>.

D.J. Wilkinson. *Stochastic Modelling for Systems Biology, Third Edition*, volume 1. Taylor & Francis Ltd, 2018.

REFERENCES

Giovanni Barone-Adesi and Robert E Whaley. Efficient Analytic Approximation of American Option Values. *Journal of Finance*, 42(2):301–320, June 1987. URL <https://ideas.repec.org/a/bla/jfinan/v42y1987i2p301-20.html>.

Kaushik Bhattacharya, Bamdad Hosseini, Nikola B Kovachki, and Andrew M Stuart. Model reduction and neural networks for parametric pdes. *arXiv preprint arXiv:2005.03180*, 2020.

Tristan Buckmaster and Vlad Vicol. Convex integration and phenomenologies in turbulence. 2019.

Ilya Chevyrev, Andris Gerasimovics, and Hendrik Weber. Feature engineering with regularity structures. 2021.

M. Hairer. A theory of regularity structures. *Invent. Math.*, 198(2):269–504, 2014.

Martin Hairer. Regularity structures and the dynamical ϕ_3^4 model. 2015.

K. Hasselmann. Stochastic climate models part i. theory. *Tellus*, 28(6):473–485, 1976. doi: 10.3402/tellusa.v28i6.11316. URL <https://doi.org/10.3402/tellusa.v28i6.11316>.

Nikola B. Kovachki, Zongyi Li, Burigede Liu, Kamyar Azizzadenesheli, Kaushik Bhattacharya, Andrew M. Stuart, and Anima Anandkumar. Neural operator: Learning maps between function spaces. *CoRR*, abs/2108.08481, 2021. URL <https://arxiv.org/abs/2108.08481>.

Zongyi Li, Nikola Kovachki, Kamyar Azizzadenesheli, Burigede Liu, Andrew Stuart, Kaushik Bhattacharya, and Anima Anandkumar. Multipole graph neural operator for parametric partial differential equations. *Advances in Neural Information Processing Systems*, 33:6755–6766, 2020a.

Zongyi Li, Nikola B. Kovachki, Kamyar Azizzadenesheli, Burigede Liu, Kaushik Bhattacharya, Andrew M. Stuart, and Anima Anandkumar. Fourier neural operator for parametric partial differential equations. *CoRR*, abs/2010.08895, 2020b. URL <https://arxiv.org/abs/2010.08895>.

Lu Lu, Pengzhan Jin, and George Em Karniadakis. Deeponet: Learning nonlinear operators for identifying differential equations based on the universal approximation theorem of operators. *arXiv preprint arXiv:1910.03193*, 2019.

Nicholas H Nelsen and Andrew M Stuart. The random feature model for input-output maps between banach spaces. *SIAM Journal on Scientific Computing*, 43(5):A3212–A3243, 2021.

Ravi G Patel, Nathaniel A Trask, Mitchell A Wood, and Eric C Cyr. A physics-informed operator regression framework for extracting data-driven continuum models. *Computer Methods in Applied Mechanics and Engineering*, 373:113500, 2021.

Cristopher Salvi and Maud Lemercier. Neural stochastic partial differential equations. *CoRR*, abs/2110.10249, 2021. URL <https://arxiv.org/abs/2110.10249>.

G. E. Uhlenbeck and L. S. Ornstein. On the theory of the brownian motion. *Phys. Rev.*, 36:823–841, Sep 1930. doi: 10.1103/PhysRev.36.823. URL <https://link.aps.org/doi/10.1103/PhysRev.36.823>.

D.J. Wilkinson. *Stochastic Modelling for Systems Biology, Third Edition*, volume 1. Taylor & Francis Ltd, 2018.

A APPENDIX

A.1 MODEL FEATURE VECTORS

We review the method to generate the *model feature vectors* introduced in Chevyrev et al. (2021). The two types of initial signals are the *forcing* ξ and functions $\{u^i\}_{i \in \mathcal{J}}$ derived from initial conditions, where \mathcal{J} is the initial index set. Usually, $u^i = I_i[u_0]$, where I_i is a linear operator determined by the specific form of equations. For the SPDE in Eqn.(1) in the main paper, $\mathcal{J} = c$ and $u^c = I_c[u_0]$.

Fix the *height* $n \in \mathbb{N}$ and the coefficient $\alpha = (m, l, p, q) \in \mathbb{N}^4$. Then the *model* \mathcal{M}_α^n of (u^i, ξ) is defined inductively by

$$\mathcal{M}_\alpha^0 = \{u^i\}_{i \in \mathcal{J}}, \quad (10)$$

$$\mathcal{M}_\alpha^n = \{I[\xi^j \prod_{i=1}^k \partial^{\mathbf{a}} f] : f \in \mathcal{M}_\alpha^{n-1}, \mathbf{a} \in \mathbb{N}^d, |\mathbf{a}| \leq q, j, k \in \mathbb{N}, 0 \leq j \leq p, 1 \leq k + j \leq m \mathbf{1}_{j=0} + l \mathbf{1}_{j>0}\} \cup \mathcal{M}_\alpha^{n-1}, \quad (11)$$

where $\mathbf{a} = (a_1, \dots, a_d)$, $\partial^{\mathbf{a}} = \partial_1^{a_1} \cdots \partial_d^{a_d} = \frac{\partial^{a_1}}{\partial x_1^{a_1}} \cdots \frac{\partial^{a_d}}{\partial x_d^{a_d}}$, $|\mathbf{a}| = \sum_{i=1}^d a_i$, m is the *additive width*, l is the *multiplicative width*, p is the *forcing order* and q is the *differentiation order*. The more specific application differs across SPDEs, and is provided in the following.

To avoid the number of model feature vectors grows exponentially, we constraint it with the *degree* function, that is, only elements do not exceed a certain degree will be involved. The degree $\deg: \mathcal{M}_\alpha^n \rightarrow \mathbb{R}$ satisfies

$$\deg I[f] = \beta + \deg f, \quad \deg \partial^{a_i} f = \deg f - |a_i|, \quad \deg \prod_{i=1}^k f = \prod_{i=1}^k \deg f, \quad (12)$$

where β is up to the operator I . The degree function is defined corresponding to the regularity. For the space-time noise ξ on $[0, T] \times D \in \mathbb{R}^d$, its Hölder regularity is $-\epsilon - (d+2)/2$ for any small $\epsilon > 0$, so we define $\deg \xi = -(d+2)/2$. (Chevyrev et al., 2021)

To help understand the rule of generating models, we provide the elements of models in the three experiments. All the operators I and I_c below have been defined as the ones in the experiment section. And for the 2d equation, we use the I_i, I_{c_i} to denote $\partial I / \partial x_i, \partial I_c / \partial x_i$ respectively, where $i = 1, 2$.

1. Dynamic ϕ_1^4 model: We note that β in (12) is 2 according to the definition of I . As for α , we take the forcing order $p = 1$ because the forcing ξ only appears once. As μ and σ do not depend on ∂_i , we take the differentiation order $q = 0$. We construct a model with additive width $m = 3$, multiplicative width $l = 1$, i.e. $\alpha = (3, 1, 1, 0)$, and degree ≤ 7.5 .
 - (a) $n = 2 : I[\xi], I_c[u_0], I[I[\xi]], I[I_c[u_0]], I[(I_c[u_0])^2], I[(I_c[u_0])(I[\xi])], I[(I[\xi])^2], I[(I_c[u_0])^2(I[\xi])], I[(I_c[u_0])(I[\xi])^2], I[(I[\xi])^3]$.
 - (b) $n = 3 : I[\xi], I_c[u_0], I[I[\xi]], I[I_c[u_0]], I[(I_c[u_0])^2], I[(I_c[u_0])(I[\xi])], I[(I[\xi])^2], I[(I_c[u_0])^2(I[\xi])], I[(I_c[u_0])(I[\xi])^2], I[(I[\xi])^3], I[I[I[\xi]]], I[I[I_c[u_0]]], I[I[(I_c[u_0])^2]], I[I[(I_c[u_0])(I[\xi])^2]], I[I[(I_c[u_0])^3]], I[I[(I_c[u_0])(I[\xi])^3]], I[I[(I_c[u_0])(I[\xi])^2]], I[I[(I_c[u_0])^2(I[\xi])^2]], I[I[(I_c[u_0])^3(I[\xi])^2]], I[I[(I_c[u_0])(I[\xi])^2(I[\xi])^2]], I[I[(I_c[u_0])^2(I[\xi])^3]], I[I[(I_c[u_0])^2(I[\xi])^2(I[\xi])^2]], I[I[(I_c[u_0])^2(I[\xi])^3(I[\xi])^2]], I[I[(I_c[u_0])^2(I[\xi])^2(I[\xi])^3]], I[I[(I_c[u_0])^2(I[\xi])^2(I[\xi])^2(I[\xi])^2]], I[I[(I_c[u_0])^2(I[\xi])^2(I[\xi])^3(I[\xi])^2]], I[I[(I_c[u_0])^2(I[\xi])^2(I[\xi])^2(I[\xi])^2(I[\xi])^2]], I[I[(I_c[u_0])^2(I[\xi])^2(I[\xi])^2(I[\xi])^3(I[\xi])^2]], I[I[(I_c[u_0])^2(I[\xi])^2(I[\xi])^2(I[\xi])^2(I[\xi])^2(I[\xi])^2]]$.
2. Parabolic equation with multiplicative forcing: As the form of this equation is almost the same as the Φ_1^4 model, the model \mathcal{M} can be constructed similarly: the operator I , the initial index set \mathcal{J} and u^c are all same. What differs is the α because the change of the forcing term. Due to the multiplicative forcing, the multiplicative width $l = 2$, i.e. $\alpha = (3, 2, 1, 0)$. Only elements whose degrees do not exceed 7.5 are involved as well.
 - (a) $n = 2 : I[\xi], I_c[u_0], I[I[\xi]], I[I_c[u_0]], I[\xi(I[\xi])], I[\xi(I_c[u_0])], I[(I[\xi])^2], I[(I[\xi])(I_c[u_0])], I[(I[\xi])^3], I[(I[\xi])^2(I_c[u_0])]$.
 - (b) $n = 3 : I[\xi], I_c[u_0], I[I[\xi]], I[I_c[u_0]], I[\xi(I[\xi])], I[\xi(I_c[u_0])], I[(I[\xi])^2], I[(I_c[u_0])(I[\xi])], I[(I[\xi])^3], I[(I_c[u_0])(I[\xi])^2], I[I[I[\xi]]], I[I[I_c[u_0]]], I[I[\xi(I_c[u_0])]], I[I[\xi(I[\xi])]], I[I[(I_c[u_0])(I[\xi])^2]], I[I[(I_c[u_0])^3]], I[I[\xi(I_c[u_0])^3]], I[\xi(I[(I[\xi])^3])], I[\xi(I_c[u_0])^3]], I[\xi(I[I[\xi]])], I[\xi(I[(I_c[u_0])(I[\xi])^2])], I[\xi(I[(I_c[u_0])^2(I[\xi])^2])], I[\xi(I[(I_c[u_0])^2(I[\xi])^3])], I[\xi(I[(I_c[u_0])^2(I[\xi])^2(I[\xi])^2])], I[\xi(I[(I_c[u_0])^2(I[\xi])^2(I[\xi])^3])], I[\xi(I[(I_c[u_0])^2(I[\xi])^2(I[\xi])^2(I[\xi])^2])], I[\xi(I[(I_c[u_0])^2(I[\xi])^2(I[\xi])^3(I[\xi])^2])], I[\xi(I[(I_c[u_0])^2(I[\xi])^2(I[\xi])^2(I[\xi])^2(I[\xi])^2])]$.
3. 2d stochastic Navier-Stokes equation: We construct the model \mathcal{M} with $\alpha = (2, 1, 1, 1)$, $\deg \leq 7.5$. As for the α , we note that the right side of the NSE contains ∇ , so the differentiation order is set to $q = 1$.

(a) $n = 2 : I[\xi], I_c[\omega_0], I[I[\xi]], I[I_1[\xi]], I[I_2[\xi]], I[I_c[\omega_0]], I[I_{c_1}[\omega_0]], I[I_{c_2}[\omega_0]], I[(I_c[\omega_0])^2], I[(I_c[\omega_0])(I_{c_2}[\omega_0])], I[(I_c[\omega_0])(I_{c_1}[\omega_0])], I[(I_c[\omega_0])(I_2[\xi])], I[(I_c[\omega_0])(I[\xi])], I[(I_c[\omega_0])(I_1[\xi])], I[(I_{c_2}[\omega_0])^2], I[(I_{c_2}[\omega_0])(I_{c_1}[\omega_0])], I[(I_{c_2}[\omega_0])(I_2[\xi])], I[(I_{c_2}[\omega_0])(I[\xi])], I[(I_{c_2}[\omega_0])(I_1[\xi])], I[(I_{c_1}[\omega_0])^2], I[(I_{c_1}[\omega_0])(I_2[\xi])], I[(I_{c_1}[\omega_0])(I[\xi])], I[(I_{c_1}[\omega_0])(I_1[\xi])], I[(I_2[\xi])^2], I[(I_2[\xi])(I[\xi])], I[(I_2[\xi])(I_1[\xi])], I[(I[\xi])^2], I[(I[\xi])(I_1[\xi])], I[(I_1[\xi])^2].$

(b) $n = 3 : I[\xi], I_c[\omega_0], I[I[\xi]], I[I_1[\xi]], I[I_2[\xi]], I[I_c[\omega_0]], I[I_{c_1}[\omega_0]], I[I_{c_2}[\omega_0]], I[(I_c[\omega_0])^2], I[(I_c[\omega_0])(I_{c_1}[\omega_0])], \dots, I[(I[(I_1[\xi])(I_2[\xi])])(I[(I_1[\xi])(I[\xi])])], I[(I[(I_1[\xi])(I_2[\xi])])(I[(I_1[\xi])(I_2[\xi])])], I[(I[(I_1[\xi])(I_2[\xi])])(I[(I_1[\xi])(I_{c_2}[\omega_0])])], I[(I[(I_1[\xi])(I_2[\xi])])(I[(I_{c_1}[\omega_0])(I[\xi])])], I[(I[(I_c[\omega_0])(I[\xi])])(I[(I_1[\xi])(I[\xi])])], I[(I[(I_{c_1}[\omega_0])^2])(I[(I_1[\xi])(I[\xi])])], I[(I[(I_1[\xi])(I[\xi])])^2], I[(I[(I_1[\xi])(I[\xi])])(I[(I_{c_1}[\omega_0])(I_{c_2}[\omega_0])])], I[(I[(I_1[\xi])(I[\xi])])(I[(I_{c_1}[\omega_0])(I_{c_2}[\omega_0])])^2], I[(I[(I_1[\xi])(I_{c_2}[\omega_0])])(I[(I_{c_1}[\omega_0])(I[\xi])])].$

A.2 OTHER BASELINES

Apart from the FNO and NSPDE, we also compare NORS with other models on the first two experiments. The complete results are report in Table 4 and Table 5, from which we can see the superiority of NORS.

Table 4: **Dynamic Φ_1^4 model.** We consider the $l2$ error of the baselines and our model($\alpha = (3, 1, 1, 0)$, $\text{deg} \leq 7.5$, $n = 2$ or 3) in two settings.

Model	$N = 1000$		$N = 10000$	
	$\xi \mapsto u$	$(u_0, \xi) \mapsto u$	$\xi \mapsto u$	$(u_0, \xi) \mapsto u$
NCDE	0.112	0.127	0.056	0.072
NRDE	0.129	0.150	0.070	0.083
NCDE-FNO	0.071	0.066	0.066	0.069
DeepONet	0.126	\times	0.061	\times
FNO	0.032	0.030	0.027	0.024
NSPDE	0.009	0.012	0.006	0.006
Ours($n = 3$)	0.0003	0.0011	0.0002	0.0004
Ours($n = 2$)	0.0002	0.0012	0.0002	0.0004

Table 5: **Parabolic equation with multiplicative forcing.** We compare the $l2$ error of the baselines and our model($\alpha = (3, 2, 1, 0)$, $\text{deg} \leq 7.5$, $n = 2$ or 3) in two settings.

Model	$N = 1000$		$N = 10000$	
	$\xi \mapsto u$	$(u_0, \xi) \mapsto u$	$\xi \mapsto u$	$(u_0, \xi) \mapsto u$
NCDE	0.016	0.087	0.010	0.059
NRDE	0.023	0.584	0.023	0.641
NCDE-FNO	0.015	0.034	0.017	0.019
DeepONet	0.023	\times	0.023	\times
FNO	0.0036	0.0063	0.0035	0.0037
NSPDE	0.0016	0.0062	0.0012	0.0026
Ours($n = 3$)	0.0006	0.0005	0.0005	0.0003
Ours($n = 2$)	0.0006	0.0006	0.0005	0.0003